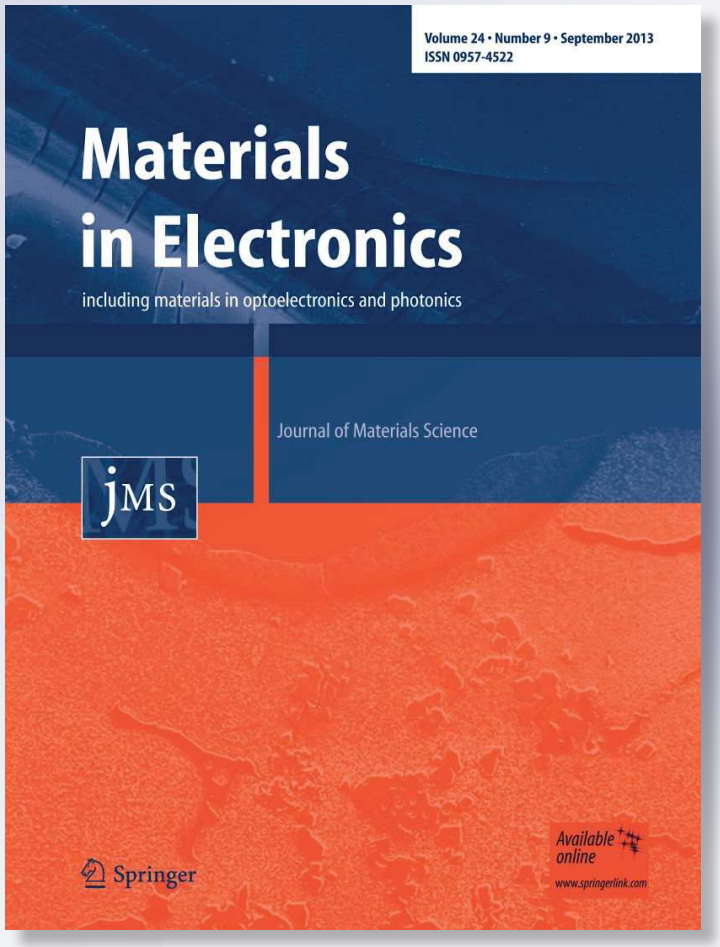
Wideband microwave absorption in thin nanocomposite films induced by a concentration gradient of mixed carbonaceous nanostructures

R. Jaiswar, C. Bailly, S. Hermans, J. P. Raskin & I. Huynen

Journal of Materials Science: Materials in Electronics

ISSN 0957-4522
Volume 30
Number 21

J Mater Sci: Mater Electron (2019)
30:19147-19153
DOI 10.1007/s10854-019-02271-3



Springer

Your article is protected by copyright and all rights are held exclusively by Springer Science+Business Media, LLC, part of Springer Nature. This e-offprint is for personal use only and shall not be self-archived in electronic repositories. If you wish to self-archive your article, please use the accepted manuscript version for posting on your own website. You may further deposit the accepted manuscript version in any repository, provided it is only made publicly available 12 months after official publication or later and provided acknowledgement is given to the original source of publication and a link is inserted to the published article on Springer's website. The link must be accompanied by the following text: "The final publication is available at link.springer.com".

Springer

Author's personal copy

Journal of Materials Science: Materials in Electronics (2019) 30:19147–19153
https://doi.org/10.1007/s10854-019-02271-3

Wideband microwave absorption in thin nanocomposite films induced by a concentration gradient of mixed carbonaceous nanostructures

R. Jaiswar[1] · C. Bailly[2] · S. Hermans[3] · J. P. Raskin[1] · I. Huynen[1]

Received: 3 June 2019 / Accepted: 23 September 2019 / Published online: 8 October 2019
© Springer Science+Business Media, LLC, part of Springer Nature 2019

Abstract
Absorption in excess of 90% is induced over a 22 GHz bandwidth by the combination of carbon nanotubes (CNTs) and graphene nanoplatelets (GNPs) dispersed in a polymer matrix. This performance is achieved by a stack of polymer films showing a concentration gradient of mixed CNTs and GNPs from layer to layer, having a total thickness of only 0.76 $\lambda/4$. Excellent agreement is observed from 18 to 40 GHz between the predicted and measured reflectivity and the resulting high absorption.

1 Introduction

Carbon-based nanostructures such as carbon nanotubes (CNTs) and graphene have been widely used for applications in electronics, specially related to (bio)sensors [1–3, 4–7], fuel cell electrodes and supercapacitors [8–10]. In all these applications the interaction between carbon structures and (bio)electrical signals is exploited to create novel devices showing enhanced performances. Another kind of interaction has been recently exploited to counteract detrimental effects of electromagnetic (EM) waves. Indeed, extensive use of wireless electronics and telecommunication devices in our daily life is the cause of increasing EM pollution and undesirable radiative effects on electronic equipment as well as, potentially, on human health. Carbon nanofillers (CNFs) such as nanotubes (CNTs) and graphene nanoplatelets (GNPs) have been shown to hold great potential as modifiers in polymer materials thanks to their exceptional across the board properties, leading to numerous avenues for applications in the electronics and materials fields.

In order to achieve thin, light-weight, and low-cost materials reducing EM pollution, polymer nanocomposites (PNCs) loaded with various types of CNFs have been extensively researched. They are typically configured as single or multilayer-stacked microwave absorbing materials (MAMs). In [11, 12], various MAMs are studied, where CNFs, including carbon black (CB), incorporated at different concentration levels in single as well as multilayer PNC configurations, induce reflection below −10 dB, albeit in a narrow frequency band. Multilayer configurations of PNCs containing a single type of inclusion such as micrometric graphite and CNFs (single- and multi-wall nanotubes or nanofibers) designed with the help of optimization algorithms show good EM absorption from 2 to 18 GHz and at various incident angles with a tradeoff in absorber thickness [13–15]. In addition, limited studies have been reported on a multilayer stack of PNCs containing combinations of CNFs, in particular about their effect on the EM parameters (permittivity ε, conductivity σ) needed to achieve thin high frequency absorbers [16, 17] using gradient concentration of nanofillers in the multilayer [18, 19].

In this paper, we first study the morphology and EM properties of CNFs individually or jointly dispersed in polycarbonate (PC) thin films. We show how these films can be stacked in a gradient concentration of CNFs in order to form a multilayered structure favoring broadband absorption, exceeding 90% over a 22 GHz bandwidth. The experimental characterization of the multilayer shows an excellent agreement with simulations used for its design.

Electronic supplementary material The online version of this article (https://doi.org/10.1007/s10854-019-02271-3) contains supplementary material, which is available to authorized users.

✉ I. Huynen
isabelle.huynen@uclouvain.be

[1] ICTEAM Institute, ELEN Division, Université catholique de Louvain (UCLouvain), 3 place du Levant, 1348 Louvain-la-Neuve, Belgium

[2] IMCN Institute, BSMA Division, UCLouvain, place Croix du sud 1, 1348 Louvain-la-Neuve, Belgium

[3] IMCN Institute, MOST Division, UCLouvain, 1 place Lavoisier, 1348 Louvain-la-Neuve, Belgium

Author's personal copy

2 Materials and methods

2.1 Fabrication of PNCs

CNTs (NC7000) were purchased from Nanocyl and GNPs (TIMREX C-Therm 002) were provided by TIMCAL, while PC Makrolon OD2015 resin pellets were purchased from Bayer. Before processing, PC pellets were dried for 24 h at 80 °C in vacuo to remove any water residues which can degrade the polymer and induce unwanted effects on the electrical and mechanical properties. The polymer–nanofiller dry-blends were compounded in a DSM Xplore microcompounder at 260 °C and 150 rpm for 15 min after a feeding time of 1–2 min. The CNTs and GNPs were separately or jointly dispersed in PC at various weight concentrations and ratios, as follows : CNTs alone at 0.5, 1, 2, or 3 wt%; GNPs alone at 1, 2.5, 5, or 10 wt%; GNPs + CNTs jointly at [(0.5, 1, or 2 wt%) + (1, 2.5, 5, or 10 wt%)]. Afterwards the extrudates were hot pressed for 2 min at 260 °C and 10 MPa using a hydraulic press, into 400 µm-thick flat sheets and finally annealed at 150 °C for 5 h and cold pressed before characterization [20].

2.2 Morphological characterisation

The transmission electron microscope (TEM) instrument used for imaging was a LEO 922 operating at 120 kV.

SEM pictures were performed on the cross-section of samples with a semi-inlens secondary electron detector using a JEOL FEG SEM 7600F operating at 2 keV. Cross-sections were obtained by cryofracture and then coated with an 8 nm chromium layer (Cressington sputter 208HR).

X-ray spectroscopy coupled with scanning electronic microscopy analyses were performed on composites film samples (without preparation) using a JEOL FEG SEM 7600F equipped with an EDX system (JEOL JSM2300 with a resolution < 129 eV) operating at 15 keV with a working distance of 8 mm. The acquisition time for the chemical spectra is 200 s with a probe current of 1 nA.

Raman spectroscopy was performed with a LabRAM HR instrument from Horiba Scientific which combines a very high spectral and spatial resolution with the ability to probe samples with three different laser wavelengths: 488 nm, 514 nm and 633 nm.

2.3 Microwave characterisation

To retrieve the dielectric constant ε and conductivity σ of the fabricated PNC samples, we used an Agilent N5247A PNA-X vector network analyzer to measure the scattering S parameters S_{11} and S_{21} through a waveguide method with the help of a TRL calibration. The measurement configuration is illustrated in Fig. 1. The sample was sandwiched between waveguide ports connected to the vector network analyzer via coaxial cables. TRL calibration moves the reference planes for the characterisation at input and output interfaces of the absorber. Finally, the absorption performance of multilayer PNCs was measured in the K and Ka-bands using waveguide method [21]. The data were averaged over three to five measurements and smoothed to reduce uncertainty. In order to retrieve the effective permittivity ε_e of a composite slab, the measured scattering parameters (S_{11}, S_{21}), namely the reflection and transmission coefficients, respectively, were related to the effective permittivity ε_e of the PNC sample:

$$z = \pm\sqrt{\frac{(1+S_{11})^2 - S_{21}^2}{(1-S_{11})^2 - S_{21}^2}}, \tag{1}$$

$$\Gamma = \frac{z+1}{z-1}, \tag{2}$$

$$\varepsilon_e = \varepsilon - \jmath\,\sigma/(2\pi f\varepsilon_o) = \frac{1}{z^2}. \tag{3}$$

In the above equations, d is the thickness of PNC sample, ε and σ are its dielectric constant and conductivity, respectively, while f is the operating frequency, ε_o is the permittivity of vacuum, and z is the normalized impedance at input of the PNC sample.

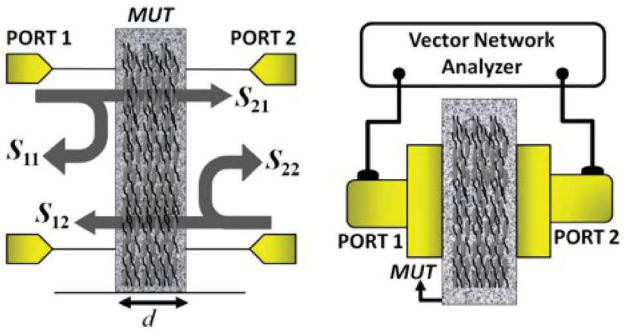


Fig. 1 Measurement configuration showing the material under test, i.e. the PNC or microwave absorbing material, inserted between rectangular waveguide ports

Author's personal copy

3 Results and discussion

3.1 Characterisation of PNC samples

3.1.1 Morphological characterisation

Figure 2 shows the TEM images of cross-sectional morphology of selected PNCs (80 nm-thick ultramicrotomes) containing different loadings of CNT and GNPs in the PC matrix. From Fig. 2, it can be seen that CNTs form an entangled interconnected conductive network throughout the PC matrix due to their 1D shape and uniform distribution. This mainly impacts the PNC conductivity, which gradually increases with the loading rate, as will be shown in Fig. 6. By opposition, GNPs show a good spatial distribution but lack the ability to form a connected network and behave more as capacitive-like structures which mainly contribute to the dielectric constant of the PNC. When both CNTs and GNPs are distributed homogeneously in the PC hosting matrix, a synergy between the 1D-tubular and 2D-planar structures yields an interconnected network even at low concentration.

Figure 3 shows SEM images of the same three samples. Figure 3a is the sample with only CNT as nanofillers, which are clearly visible as bright curled filaments. Figure 3b is the sample with only graphenic inclusions, where the flakes are also clearly visible. The mixed sample (Fig. 3c) displays again clearly the graphenic flakes but the carbon nanotubes are more difficult to distinguish at the lower resolution of SEM images.

Figure 4 shows the EDX spectrum of sample CNT0.5% to +GNP5%. As expected, peaks associated to carbon and oxygen are clearly identified, confirming the composites chemical composition. EDX spectra of various samples and different magnification ranges are available in ESM, Sect. 1.

Finally, Raman spectroscopy was performed on samples CNT2%, GNP10%, and CNT0.5% + GNP5%. They are shown in ESM, Sect. 2, as useful additional information. As expected peaks attributable to both the PC polymer matrix [22] and nanocarbon inclusions [23] are visible.

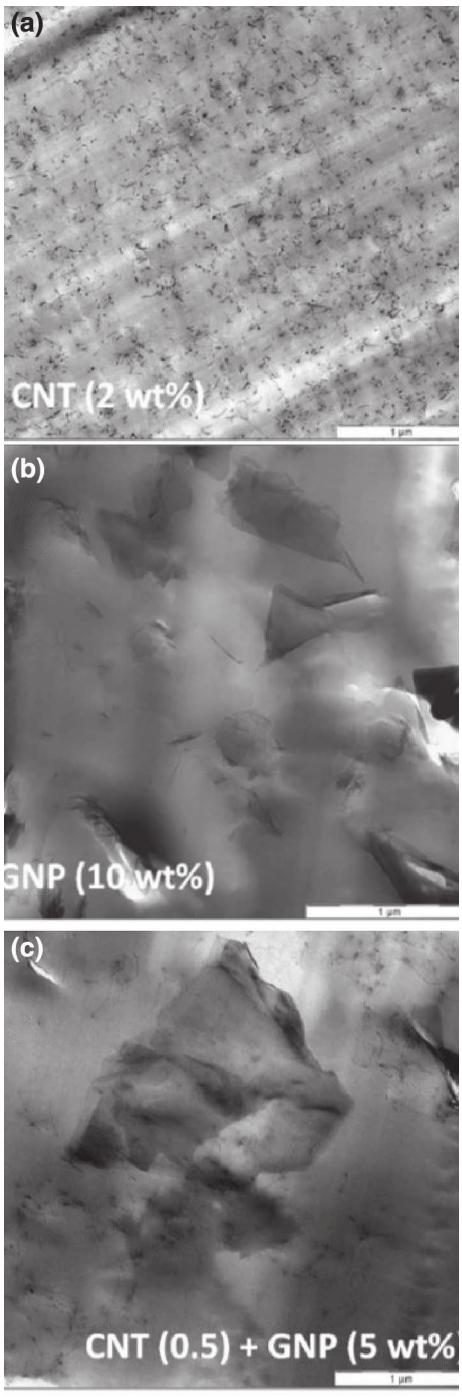


Fig. 2 TEM micrographs of fabricated nanocomposites loaded with conductive nanofillers, **a** CNT (2 wt%), **b** GNPs (10 wt%) and **c** CNT + GNP (0.5 wt% + 5 wt%) in polycarbonate matrix. Scale bar is 1 μm

3.1.2 Microwave electrical parameters

Figures 5 and 6 show the measured dielectric constant ε and conductivity σ of the PNCs at different loading of CNTs and GNPs in the matrix, either alone or mixed at the above-reported concentrations. The composites loaded with CNTs only (red curves) show an excellent increasing conductivity trend between 1 and 29 S/m as the filler concentration is increased from 0.5 to 3 wt%. By opposition, their dielectric constant grows quickly from the value for pure PC equal to 2.9 but begins to saturate around 15 at 3 wt% after a moderate increment from 0.5 to 2 wt% CNT concentration. On the contrary, PNCs loaded with GNP only (brown curves) show a linear increment of the

Author's personal copy

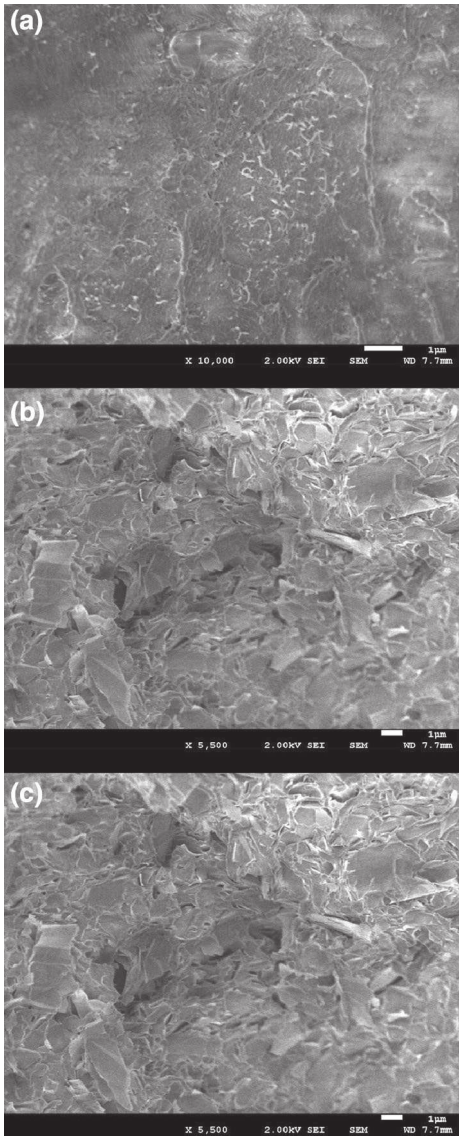


Fig. 3 SEM micrographs of nanocomposites loaded with conductive nanofillers, **a** CNT (2 wt%), **b** GNPs (10 wt%) and **c** CNT + GNP (0.5 wt% + 5 wt%) in polycarbonate matrix. Scale bar is 1 μm

dielectric constant up to 23 when the filler concentration increases from 1 to 10 wt% but their conductivity only increases slowly due to poor nanofiller connectivity. It is clear from Figs. 5 and 6 and also from TEM micrographs in Fig. 2 that CNTs and GNPs dispersed in polymer, have very different influences on the conductivity and dielectric constant of the PNCs due to their specific geometrical shape. However, increasing either individual loadings of CNTs or GNPs will make the material processing very difficult and the flexibility of the composite will be compromised, which limits its utilization. On the other hand, the hybrid concept of blending CNTs and GNPs together in a polymer matrix and further taking advantage of a CNF

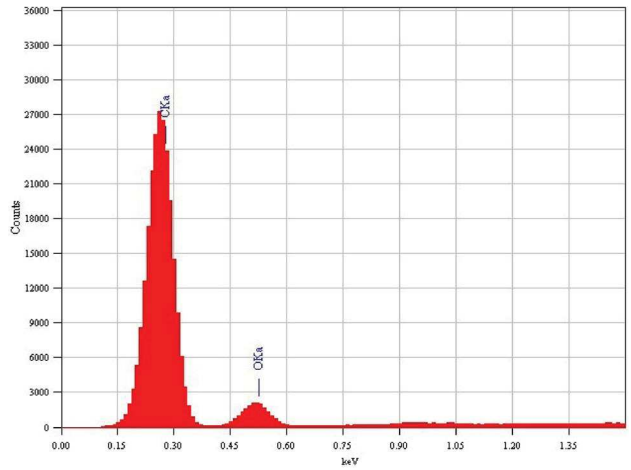


Fig. 4 EDX spectrum of sample CNT2% + GNP5%

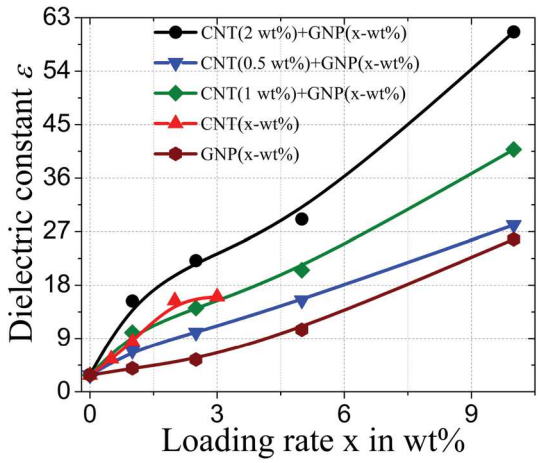


Fig. 5 Dielectric constant ε_r extracted at 23 GHz from measurement of S-parameters of prepared composite slabs

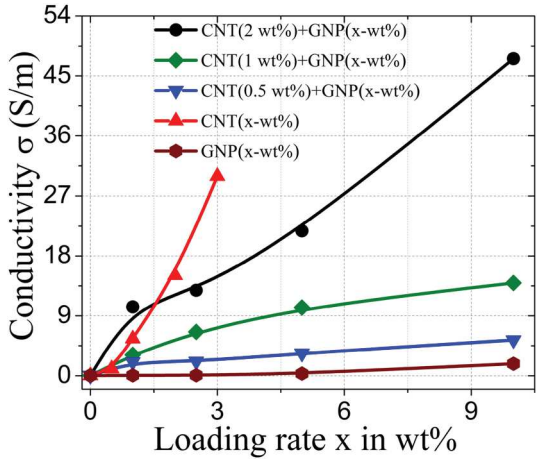


Fig. 6 Conductivity σ extracted at 23 GHz from measurement of S-parameters of prepared PNC slabs

Author's personal copy

concentration gradient through the structure hopefully allows to synergistically increase the conductivity and dielectric constant. *This is the basic idea for the design of the proposed multilayered MAM in the present paper*. The measured conductivity of hybrid CNT + GNPs PNCs indeed lies between the conductivity of the composites reinforced with a single nanofiller, CNT or GNP, at a given concentration. The conductive nanofiller network in CNT and GNP nanocomposites can be understood as the end-to-end or overlapped interconnection formed between CNT–CNT, CNT–GNP, GNP–GNP throughout the polymer matrix as illustrated in Fig. 7.

The formation of an interconnected conductive network through micro- and nano-aggregates of nanofillers, significantly impacts the AC conductivity and dielectric constant in PC–CNT–GNP composites, which may be attributed to the following reasons [24]. Firstly, CNTs serve as bridges connecting GNPs and help form a continuous network of fillers in the PNCs, responsible for the conductivity σ. Secondly, the 2D aspect ratio of GNPs hampers the hopping of electrical charges between the CNTs and the stacked sheets act as capacitances associated to the dielectric constant ε.

Indeed, the formation of active conductive branches and bridges between CNTs and GNPs is established either through end-to-end connection or overlapped nano-fillers, making the conduction pathways between discrete islands (micro- and nano-aggregates) of nanofillers inside the polymer matrix [25, 26]. As the loading of the nanofillers increases, the tunneling distance reduces and the number of contact points increases, which contributes to increasing the bulk conductivity of the nano-composite.

3.2 Microwave absorbing material

3.2.1 Design

The design of the MAM is achieved through a transmission-line approach and the design constraints are as follows:

(1) Reflectivity must be < -10 dB or absorption is $> 90\%$ in the whole frequency range (18–40 GHz);
(2) Minimal number of layers in the multilayered nanocomposite;
(3) Minimal total thickness of the nanocomposite, i.e. < 4.2 mm, quarter wavelength at 18 GHz.

Overall, the gradual increase in conductivity σ and permittivity ε of the various substrates in the multilayer provides higher microwave absorption in the ultra-wide frequency band. The choice of composition and number of layers can be optimized taking into account available material properties, thickness limit and operational bandwidth. The designed multilayer nanocomposite having graded concentration facilitates the step-by-step attenuation of the wave propagating inside the multilayered lossy medium and results in wideband absorption [27] at reduced thickness.

The MAM is constructed from nanocomposites reported in Figs. 5 and 6, arranged in a gradient composition cascade, as depicted in the inset of Fig. 9. Table 1 provides the parameters of the constitutive nanocomposite layers. It is observed from Table 1 that the EM properties (ε, σ) increase from the air–absorber interface up to the grounded plane (similar to tapered line impedance distribution) so that the wave can penetrate from the top lower permittivity layer inside the lossy medium and is absorbed when propagating throughout the absorber.

The reflection at input and transmission through the MAM are formulated using a chain matrix approach. The chain matrix of layer i, noted T_i expresses as:

$$T_i = \begin{bmatrix} \cosh(\gamma_i d_i) & Z_{ci}\sinh(\gamma_i d_i) \\ 1/Z_{ci}\sinh(\gamma_i d_i) & \cosh(\gamma_i d_i) \end{bmatrix} \quad (4)$$

with $\gamma_i = \jmath\, 2\pi f\sqrt{\varepsilon_{ei}}\,/c_o, Z_{ci} = 377\Omega/\sqrt{\varepsilon_{ei}}$, where ε_{ei} is the permittivity of layer i from (1d), and d_i its thickness

Table 1 Nomenclature, composition and electromagnetic parameters of the five layers forming the MAM

	Composition	d (mm)	ε	σ (S/m)
1	Neat PC	1.2	2.9	0.037
2	CNT(0.5 wt%) + GNP(1 wt%)	0.4	5	2.068
3	CNT(1 wt%) + GNP(2.5 wt%)	0.4	14.15	6.59
4	CNT(2 wt%) + GNP(1 wt%)	0.4	15.336	10.21
5	CNT(2 wt%) + GNP(5 wt%)	0.8	29.097	21.77

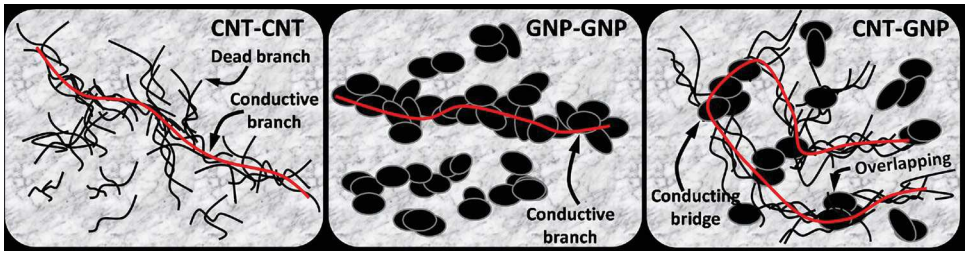


Fig. 7 Formation of co-supportive conductive nanofillers (CNT, GNPs) network in the polymer nanocomposite

Author's personal copy

according to Table 1. The global T-matrix of the MAM expresses as the product of individual layer matrices T_i:

$$T = \prod_{i=1}^{5} T_i. \tag{5}$$

The global T matrix is then converted to the corresponding S-matrix referenced to the 377Ω impedance of air, using formulas from [28]. The reflectivity R at input of the MAM and the absorption A through it are:

$$R = \left| S_{11} - \frac{{S_{21}}^2}{1 + S_{22}} \right|, \tag{6}$$

$$A = 1 - R^2. \tag{7}$$

These equations assume that the layer 5 having the highest concentration is backed by a metallic plate (PEC), as depicted in inset of Fig. 9. This configuration ensures a maximal absorption since the wave coming at the PEC after being absorbed undergoes again absorption when it is reflected back by the PEC. This configuration is used for the measurement of the MAM, involving no transmission since all the signal undergoes absorption and reflection inside the sample.

3.2.2 Experimental characterisation of the MAM

Figures 8 and 9 show the measured and simulated reflectivity R and absorption A for the MAM depicted as inset of Fig. 9. The MAM is constructed using measured nanocomposites stacked following Table 1. The simulation uses measured values of Table 1 and Eqs. (4)–(7). The absorption observed experimentally is higher than 90% from 18 GHz untill 40 GHz at least, meaning a bandwidth over 22 GHz. As well the reflectivity is lower than −10 dB over the same bandwidth.

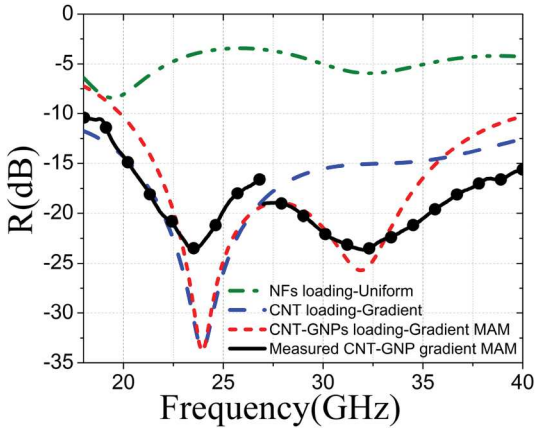


Fig. 8 Measured (solid black) and calculated (dashed red) reflectivity R of MAM, expressed in dB. Green curve corresponds to simulation performed for uniform concentration of NFs (8), and blue one is for gradient concentration of CNTs only (Color figure online)

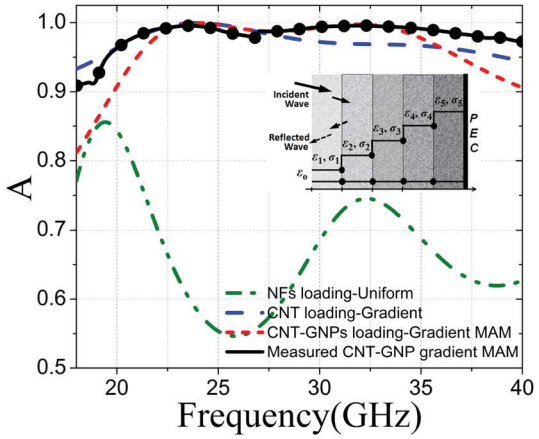


Fig. 9 Measured (solid black) and calculated (dashed red) absorption A of MAM. Green curve corresponds to simulation performed for uniform concentration of NF (8), and blue one is for gradient concentration of CNTs only. Inset shows schematic of graded-concentration construction of MAM (Color figure online)

Figures 8 and 9 also illustrate the benefit of a gradient concentration and of the combination of CNTs and GNPs in PC layers. Blue curves show the performances of a MAM having layers of same thickness as in Table 1, but with parameters corresponding to the four increasing values shown for CNT only in Figs. 5 and 6 (red curves), for ε and σ, respectively. It is observed that CNTs taken alone (single filler configuration) cannot maintain the minimal reflectivity level of −20 dB, that is of special interest for sensitive applications in EMC. It corresponds to an absorption level equal to 99%. Green curves in Figs. 8, 9 show the performances of an absorber of same thickness having a uniform concentration of NFs in each layer, meaning constant values for ε_r and σ from layer to layer, taken equal to their *mean* values over thickness:

$$\varepsilon_m = \frac{\sum_{i=1}^{5} \varepsilon_i \times d_i}{\sum_{i=1}^{5} d_i}; \quad \sigma_m = \frac{\sum_{i=1}^{5} \sigma_i \times d_i}{\sum_{i=1}^{5} d_i}. \tag{8}$$

Absorption falls down, below 70%, due to a reflectivity level higher than −8 dB.

3.3 Assessment of performances

Table 2 shows the comparison in terms of bandwidth and thickness with other state-of-the-art broadband absorbers. It is evident that the proposed MAM absorber stands out in terms of absorption bandwidth and compactness, since it has the highest BW and lowest thickness.

Author's personal copy

Table 2 Comparison with MAM absorbers from literature. Exact concentration of CNT, carbon black (CB), CNT foam (CNTF) and polyaniline (PANI) are available in corresponding references

References	Matrix	Composition	d	BW
[29]	PU	CB, CNT	9.9	3
[14]	Epoxy	GNP, CNF	10	5.5
[30]	Epoxy	GNP, CNF	10	3.5
[31]	Epoxy	CNT	8.9	13
[15]	Epoxy	CNT	6.6	11
[32]	Epoxy	CNT, CNF, PANI	36.6	13
[13]	Epoxy	CNT, CNF, GNP, PANI	30.4	10
This work	PC	CNT, GNP/five layers	3.2	22

Thickness *d* is in mm and bandwidth BW is in GHz

4 Conclusion

As a conclusion the performances of the MAM agree well with the nominal specifications. The bandwidth is 22 GHz corresponding to a fractional bandwidth equal to 0.8, for a total thickness equal to 3.2 mm, corresponding to $0.76\lambda/4$ at 18 GHz. The MAM absorber outperforms the uniform and single filler solutions.

Acknowledgements The authors are grateful to the National Fund for Scientific Research (F.R.S.-FNRS, Belgium) for supporting this research. This work is also supported by the Walloon region, and by the "Communauté Française de Belgique", through the Project "Nano4waves" funded by its Research Program "Actions de Recherche Concertées". Special thanks are also due to Mr. H. Mesfin for the fabrication of the composite layers and to Professor A. Delcorte for fruitful discussions in the frame of the Nano4waves Project. The help of S. Bebelmans, D. Magnin, J. Mahy, W. Malik and P. Simon for the various characterizations was also highly appreciated.

References

1. A. Khoshroo et al., J. Electroanal. Chem. **823**, 61–66 (2018)
2. J. Amania et al., Anal. Biochem. **548**, 53–59 (2018)
3. H.R. Naderi et al., Appl. Surf. Sci. **423**, 1025–1034 (2017)
4. I.V. Zaporotskova et al., Mod. Electron. Mater. **2**, 95–105 (2016)
5. V.D.N. Bezzon et al., Adv. Mater. Sci. Eng. **4**, 1–21 (2019)
6. S. Revathia et al., Int. J. Electron. Electr. Comput. Syst. **7**, 9–16 (2018)
7. J. Pena-Bahamonde et al., J. Nanobiotechnol. **16**, 1–17 (2018)
8. G. Ijeomah et al., Int. J. Nano Biomater. **6**, 83–109 (2016)
9. L. Fekri Aval et al., Heliyon **4**, 1–17 (2018)
10. A. Bakandritsos et al., FlatChem **13**, 25–33 (2019)
11. J.-B. Kim et al., Compos. Sci. Technol. **68**, 2909 (2008)
12. J.-B. Kim, Adv. Compos. Mater. **21**, 333 (2012)
13. D. Micheli et al., IEEE Trans. Microw. Theory Tech. **59**, 2633 (2011)
14. D. Micheli et al., in *IEEE-NANO 2009. 9th IEEE Conference on Nanotechnology*, 2009
15. D. Micheli et al., Acta Astronaut. **88**, 61 (2013)
16. G. De Bellis et al., Carbon **49**, 4291 (2011)
17. A.G. D'Aloia et al., Carbon **73**, 175 (2014)
18. I. Huynen et al., in *38th European Microwave Conference (EuMC)*, ISBN 978-2-87487-006-4 (2008)
19. Y. Danlee et al., Compos. Sci. Technol. **100**, 182 (2014)
20. P. Potschke et al., Eur. Polym. J. **40**, 137 (2004)
21. N. Quiévy et al., IEEE Trans. Electromagn. Compat. **54**, 43–51 (2012)
22. V. Resta et al., Vacuum **116**, 82–89 (2015)
23. G. Sobon et al., Opt. Express **20**, 19463–19473 (2012)
24. U. Szeluga et al., Composites A **73**, 204 (2015)
25. J. Sumfleth et al., J. Mater. Sci. **44**, 3241 (2009)
26. S.M. Zhang et al., eXPRESS Polym. Lett. **6**, 159 (2012)
27. Y. Li et al., Compos. Sci. Technol. **138**, 209 (2017)
28. D. Pozar, *in Microwave Engineering*, 2nd edn. (Wiley, New York, 1998)
29. K.-Y. Park et al., Compos. Sci. Technol. **66**, 576–584 (2006)
30. D. Micheli et al., Compos. Sci. Technol. **70**, 400–409 (2010)
31. D. Micheli et al., Acta Astronaut. **69**, 747–757 (2011)
32. D. Micheli et al., Carbon **77**, 756–774 (2016)

Publisher's Note Publisher's Note Springer Nature remains neutral with regard to jurisdictional claims in published maps and institutional affiliations.